

CrossMark
click for updatesCite this: *Catal. Sci. Technol.*, 2016,
6, 8314

Nitrate–nitrite equilibrium in the reaction of NO with a Cu-CHA catalyst for NH₃-SCR†

C. Tyrsted,^a E. Borfecchia,^{*ab} G. Berlier,^b K. A. Lomachenko,^c C. Lamberti,^{bc}
S. Bordiga,^b P. N. R. Vennestrøm,^a T. V. W. Janssens,^a H. Falsig,^a
P. Beato^a and A. Puig-Molina^a

The equilibrium reaction between NO and Cu-nitrate, $\text{Cu(II)-NO}_3^- + \text{NO(g)} = \text{Cu(II)-NO}_2^- + \text{NO}_2(\text{g})$, has been proposed to be a key step in the selective catalytic reduction of NO by ammonia (NH₃-SCR) over Cu-CHA catalysts and points to the presence of Cu-nitrites. Whereas the formation of gaseous NO₂ has been observed, a direct observation of Cu-nitrite groups under conditions relevant to NH₃-SCR has been so far unsuccessful. In an effort to identify and characterize Cu-nitrites, the reaction between Cu-nitrates hosted in the CHA zeolite and NO is investigated by Fourier transform infrared spectroscopy (FTIR), ultraviolet-visible spectroscopy (UV-vis) and X-ray absorption spectroscopy (XAS). We find that NO reacts with Cu-nitrates and that about half of the Cu-nitrate species are converted. After the reaction, the Cu(II) state is different from the original oxidized state. Analysis of XAS data indicates that the final state of the Cu-CHA catalyst is consistent with the partial conversion of the Cu-nitrate species to a bidentate Cu-nitrite configuration.

Received 25th August 2016,
Accepted 12th October 2016

DOI: 10.1039/c6cy01820c

www.rsc.org/catalysis

1. Introduction

The selective catalytic reduction of NO_x by NH₃ (NH₃-SCR) plays an important role in the abatement of NO_x emission from diesel exhaust gases. The most commonly applied catalysts for this reaction are vanadium oxide and Cu- or Fe-exchanged zeolites. Recently, Cu-CHA zeolites have become more important, due to a combination of high catalytic activity and superior thermal stability.^{1–6} Knowledge on the location and coordination of copper in CHA zeolites is vital for understanding the SCR mechanism and performance and has been an avid topic in recent publications, including both experimental and theoretical results.^{7–19}

Even though the NH₃-SCR reaction over Cu-zeolites is well known, the role of the Cu and Brønsted sites and the reaction mechanism are still under debate. In the NH₃-SCR reaction, NO reacts with ammonia and oxygen to form ni-

trogen and water, according to the equation $4\text{NO} + 4\text{NH}_3 + \text{O}_2 \rightarrow 4\text{N}_2 + 6\text{H}_2\text{O}$. If NO₂ is present, NO and ammonia can also react *via* the fast SCR reaction: $2\text{NO} + 4\text{NH}_3 + 2\text{NO}_2 \rightarrow 4\text{N}_2 + 6\text{H}_2\text{O}$. Recently, a consistent reaction mechanism has been proposed for the NH₃-SCR reaction on Cu-zeolites, in which the mass balance is kept in each step, while allowing only adsorption and desorption of stable molecules.⁷ It is noted that the mechanism in question is not exhaustive, in the sense that it only describes possible reaction steps for the NH₃-SCR reactions itself but gives no explanations for several known issues of the NH₃-SCR reaction, such as influence of Cu-dimers, Brønsted sites and N₂O formation.

According to the reaction mechanism presented in ref. 7, the standard NH₃-SCR reaction is the coupling of NO activation by O₂ on a Cu(I) site to the fast SCR reaction cycle. Consequently, the fast SCR reaction is an inherent part of the standard one, and from this, it follows that the rate determining step in standard SCR is the activation of NO by O₂.

Activation of NO with O₂ leads to the formation of nitrate intermediates, which have been identified with X-ray absorption spectroscopy (XAS), electron paramagnetic resonance (EPR) and Fourier transform infrared spectroscopy (FTIR).^{7,20,21} The coupling of the NO activation to the fast SCR reaction in the mechanism cited above proceeds through the release of an NO₂ molecule, which then reacts with NO and

^a Haldor Topsøe A/S, Haldor Topsøes Allé 1, 2800 Kgs. Lyngby, Denmark^b Department of Chemistry, NIS Center and INSTM Reference Center, University of Turin, via P. Giuria 7, 10125 Turin, Italy. E-mail: elisa.borfecchia@unito.it^c IRC “Smart Materials”, Southern Federal University, Zorge Street 5, 344090 Rostov-on-Don, Russia† Electronic supplementary information (ESI) available: Evolution of FTIR bands for Cu-nitrates in NO after NO + O₂ at 100 °C; XANES spectra of Cu-CHA prior to reaction of Cu-nitrates with NO; DFT-assisted XANES simulations; details on EXAFS fitting and *k*-space analysis of experimental EXAFS spectra; EXAFS tests on hypothetical monodentate Cu(II)-NO₂ species. See DOI: 10.1039/c6cy01820c

NH₃ on another Cu(I) site, according to fast-SCR. The NO₂ molecule is formed in the reaction of NO from the gas phase with the nitrate intermediates.⁷ This reaction is known to be in equilibrium²⁰ and can be written as follows (eqn (1)):



where Z stands for the 1Al site of the zeolite framework.⁷ According to the reaction in eqn (1), some NO₂ is released in the gas phase when nitrate intermediates are exposed to NO. A transient release of NO₂ has indeed been observed,^{7,20,22,23} in line with this reaction. It is noted that the reaction in eqn (1) also leads to the formation of a Cu-nitrite species, and in the absence of ammonia and oxygen, the original state of the catalyst cannot be restored.⁷ Therefore, exposure of a Cu-nitrate species to NO alone can only result in a transient release of NO₂, as the Cu-nitrate species are depleted by the reaction.

Another way to confirm the reaction in eqn (1) as a possible part of the NH₃-SCR cycle is by a direct spectroscopic observation of the Cu-nitrite formation. This is not straightforward, due to the low thermal stability of nitrite species, also in non-reactive atmospheres.^{24–26} Recent studies on NO_x storage reduction catalysts show that nitrite species react to form nitrates in the presence of NO_x above 150 °C,²⁷ which complicates the detection of the Cu-nitrate/Cu-nitrite transformation. In NH₃-SCR, this becomes less prominent due to the high reactivity of these species for NO and NH₃ in the SCR atmosphere.²⁰ In NO oxidation over Fe-ZSM-5, an indirect trapping technique using BaO was employed to identify the presence of nitrites in the system.²⁸ This technique relies on the formation of the HNO₂ or NO₂ gas phase species and is therefore not specific for metal-nitrite formation on the catalyst.

A further complication for the detection of a nitrite species is the presence of NO₂ in the gas phase, as this will drive the equilibrium in eqn (1) towards the nitrate side. The equilibrium constant for the reaction in eqn (1) can be written as follows, $K_{\text{eq}} = p_{\text{NO}_2}/p_{\text{NO}}$, which at 200 °C has an estimated value of 3.0×10^{-6} to 3.8×10^{-5} .⁷ This means that a shift in the equilibrium to the nitrate side can already be expected when the partial pressure of NO₂ is 5–6 orders of magnitude lower than that of NO. A gas mixture of NO and O₂ will very often contain amounts of NO₂ higher than this equilibrium concentration, given the natural oxidation of NO occurring, albeit slowly, in the gas phase. Therefore, removal of O₂ from the gas mixture may result in a partial pressure of NO₂ low enough to shift the equilibrium towards the nitrite side, thus allowing for a sufficiently high conversion of Cu-nitrate to Cu-nitrite species.

Based on the proposed reaction mechanism for NH₃-SCR,⁷ we present a study aimed at the spectroscopic identification of Cu-nitrite intermediates in a Cu-CHA catalyst by exposing Cu(II)-nitrate species to NO in the absence of oxy-

gen. It is noted that these are non-steady state experiments in which we attempt to monitor a single step in the NH₃-SCR cycle. As it is known that the Cu-nitrate, and probably also Cu-nitrite, species react with ammonia to give Cu(NH₃)₂⁺ and Cu(NH₃)₄²⁺ complexes,^{7,17} a possible formation of Cu-nitrite species in detectable amounts can only be achieved in the absence of ammonia. A drawback of removing ammonia from the system is that the reaction between Cu-nitrate and NO may be affected as well and become different from the actual reaction in NH₃-SCR. However, since we want to verify if it is possible to form a Cu-nitrite species by reaction of a Cu-nitrate species with NO, we have to accept these conditions; the experiment becomes impossible otherwise.

Herein, the reaction between Cu-nitrates and NO is followed by *in situ* FTIR^{29,30} and XAS,^{31,32} in both the near edge region (XANES) and the extended region (EXAFS). XAS analysis is assisted by density functional theory (DFT) calculations, to obtain information about the local coordination geometry, ligands, and oxidation state of the Cu ions. Furthermore, complementary information is obtained from ultraviolet-visible-near infrared spectroscopy (UV-vis-NIR).^{24–26}

2. Results and discussion

Formation of nitrates on Cu-zeolites is well known upon exposure to NO₂ or the combination of NO and O₂. This can be exploited in order to directly access the hypothesized equilibrium between Cu(II)-nitrate and Cu(II)-nitrite, relevant for the NH₃-SCR reaction cycle, without having to reduce Cu(II) into Cu(I) by NH₃ and NO first.⁷ Thus, for all investigations, the Cu(II)-CHA catalyst was dehydrated in O₂ and the Cu(II)-nitrate directly prepared by exposure of the sample to a mixture of NO and O₂.

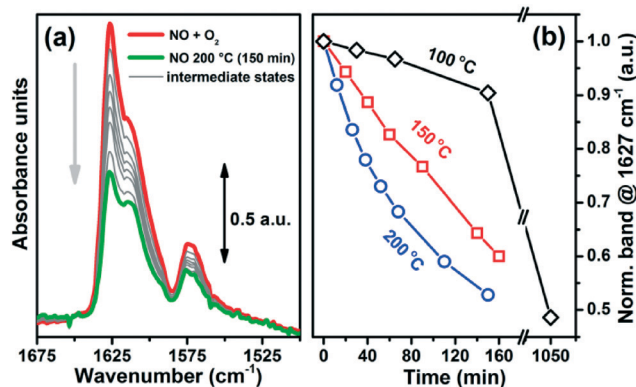


Fig. 1 (a) FTIR spectra measured on the Cu-CHA sample after oxidation in O₂ at 400 °C and exposure to a flow of NO + O₂ at 200 °C showing the conversion of Cu(II)-NO₃⁻ bands during subsequent flow in NO. (b) Normalized intensity of the 1627 cm⁻¹ FTIR band during exposure of the formed Cu(II)-NO₃⁻ in a flow of NO at 200 °C (blue curve), 150 °C (red curve) and 100 °C (black curve) for the Cu-CHA sample.

2.1 Monitoring the reaction of NO with Cu-nitrate species by FTIR

The formation of Cu-nitrates and their consecutive reaction with NO were monitored using FTIR spectroscopy. After dosing a mixture of NO and O₂ at 200 °C to the Cu-CHA catalyst, the FTIR spectrum shows three bands at 1627, 1600, and 1570 cm⁻¹, which are characteristic for the formation of a bidentate Cu-nitrate species (Fig. 1a).^{7,33} When oxygen is removed from the gas feed, the intensity of these three bands gradually decreases to about half the initial intensity at 200 °C within 150 min. At 150 °C and 100 °C, a similar decrease in intensity is observed but at a sensibly lower rate (Fig. 1b and S1, ESI†). As a control experiment, we also followed the evolution of the nitrate band intensity while flushing He at 100 °C, after their formation at 200 °C in NO + O₂. The observed trend shows a sensibly faster decrease, with respect to that reported in Fig. 1b (black curve), supporting that what is observed when changing from NO + O₂ to NO flow (a very slow decrease in the nitrate bands at this temperature) is connected to a different process with respect to simple thermal desorption.

These results demonstrate that the Cu-nitrate species reacts with NO and that the influence of temperature on the reaction rate cannot simply be ascribed to kinetics. Unfortunately, FTIR spectroscopy cannot directly confirm the formation of nitrite species, which should be formed according to eqn (1). Indeed, the characteristic nitrite FTIR bands fall in the 1470–1050 cm⁻¹ range, which in Cu-CHA is fully overshadowed by the more intense asymmetric stretching modes of the zeolite framework.^{20,27,33} Nonethe-

less, even though new FTIR features ascribable to Cu-nitrites are not observed, the conversion of the nitrates with NO is clear.

2.2 UV-vis-NIR spectrum of Cu-CHA after dehydration and reaction of Cu-nitrates with NO

Fig. 2 shows the UV-vis-NIR spectra of Cu-CHA after initial dehydration in O₂ at 400 °C and subsequent exposure to NO + O₂ at 200 °C, followed by exposure to NO at 200 °C or 100 °C. Consistently with previous studies,^{8,10} the UV-vis-NIR spectrum of the O₂-activated catalyst shows a strong absorption around 40 000 cm⁻¹, which also contains clearly distinguishable components in the region of 32 000–22 000 cm⁻¹, assigned to ligand-to-metal charge transfer (LMCT) absorption. The similarity of this feature with the electronic absorption of synthetic bis(μ-η²:η² peroxo)dicopper complexes was pointed out in previous studies;⁸ however, its conclusive assignment to dimeric copper sites still deserves further investigations. Finally, a characteristic quadruplet feature is seen in the 22 000–8500 cm⁻¹ range. This spectral region is typically associated with Cu(II) d–d transitions,^{8,10} although the unusual intensity of the quadruplet is more in line with what is typically observed for charge-transfer transitions.³⁴

Upon exposure to a mixture of NO and O₂ at 200 °C, to form the Cu(II)-nitrate species, the position and shape of the LMCT transition is modified, with an increase in intensity around 35 000 cm⁻¹ and the disappearance of the shoulder in the 32 000–22 000 cm⁻¹ region. The total absorption of the quadruplet also decreases notably and a change in shape is observed. The changes in the LMCT feature and shoulders as well as those in the 22 000–8500 cm⁻¹ region indicate a change in the local environment of a major part of the Cu(II) ions. Bands observed in the d–d region are consistent with the formation of a Cu(II)-nitrate species and closely resembles that observed by Lehnert *et al.* for homogeneous Cu(II) complexes with bidentate nitrate ligands.³⁵ When the Cu(II)-nitrate is subsequently exposed to NO at 200 °C, the shape of the LMCT transition is almost recovered above 32 000 cm⁻¹, and the total intensity in the quadruplet feature increases, concomitantly with a restoration of its original spectral shape. However, the shoulder in the range of 32 000–22 000 cm⁻¹ does not come back.

Exposure of the Cu(II)-nitrate state to NO at 100 °C yields significantly different spectral modifications with respect to what is observed at 200 °C. Firstly, the shape of the LMCT transition is very similar to that measured in the presence of the NO + O₂ mixture. Furthermore, the intensity in the d–d region strongly decreases, losing the typical quadruplet shape. The new feature is similar but not identical to the NO + O₂ state. Such a change would be consistent with partial conversion of the Cu-nitrates species into different Cu(II) moieties, with a very similar coordination geometry, as it would be expected in the case of bidentate Cu-nitrites.

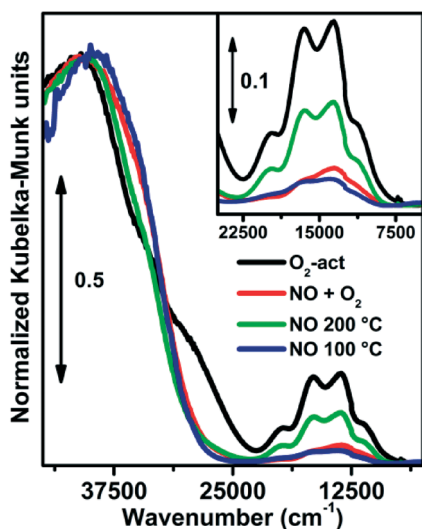


Fig. 2 UV-vis-NIR spectra measured on the Cu-CHA sample after dehydration in O₂ at 400 °C (black line), NO + O₂ flow at 200 °C (red line) and subsequent NO flow at 200 °C (green line) and 100 °C (blue line). The inset reports a magnification of the reported spectra in the 22 000–8500 cm⁻¹ range, where Cu(II) d–d transitions typically occur. The spectra were arbitrarily normalized by setting the maximum intensity to 1, to correct for changes in the overall intensity related to cell positioning in the instrument after each treatment.

In summary, UV-vis-NIR spectroscopy clearly shows that the state of the copper species from the initial dehydration in O_2 is not recovered upon exposure to $NO + O_2$ or the consecutive treatment in NO alone. In particular, the shoulder seen in the $32\,000\text{--}22\,000\text{ cm}^{-1}$ range does not reappear as the $Cu(II)$ -nitrate species are exposed to NO . Furthermore, specific temperature-dependent modifications occur in the d-d region, possibly connected to the different conversion rates of Cu -nitrates at 200 and 100 °C evidenced by FTIR and to the thermal instability of Cu -nitrite species at 200 °C.

2.3 Structural characterization of Cu -nitrates and identification of possible Cu -nitrite species by XAS

X-ray absorption spectroscopy in both XANES and EXAFS regions has been widely employed to study the structural and electronic configuration of copper ions in zeolites,^{1,6,11,31,36–43} and in the present study, it is used to characterize Cu -nitrate and possible Cu -nitrite species.

The Cu K-edge XANES spectrum observed after the initial dehydration in O_2 is characteristic for anhydrous $Cu(II)$ species in Cu -CHA catalysts.¹¹ When the $Cu(II)$ -nitrates are formed in a mixture of NO and O_2 at 200 °C, the white line intensity increases, and there is an overall flattening of the shoulders observed in the pre-edge region for the sample

dehydrated in O_2 , consistently with previously reported data⁷ (see Fig. S2, ESI†).

Conversely, the reaction of NO with the nitrate species does not strongly affect the XANES features (Fig. 3). This indicates that (i) the reaction of NO with nitrates does not restore the original O_2 -activated $Cu(II)$ state, as also evidenced by the UV-vis and FTIR experiments (Fig. 1 and 2), and (ii) the average local coordination geometry of Cu -sites is very similar before and after reaction of Cu -nitrates with NO .

To further understand the local environment and structure of the $Cu(II)$ -nitrates and identify potential $Cu(II)$ -nitrites, the geometry of these species was optimized by DFT. Several configurations were explored, including chelating bidentate $Cu(II)$ -nitrates and bidentate and monodentate $Cu(II)$ -nitrites, hosted both in the 6r and 8r ring of the CHA framework, as shown in Fig. S3, ESI†. Simulated XANES spectra were also calculated for all the DFT-optimized Cu geometries, allowing a first screening of the different candidate Cu -species and coordination environments. XANES simulations show that – when Cu -nitrate or Cu -nitrite species are formed – it would be extremely difficult to distinguish the 8r position from the possible 6r site.

This is in agreement with the recent study by McEwen and co-workers, highlighting that energetic and structural differences between the two locations are significantly lowered in

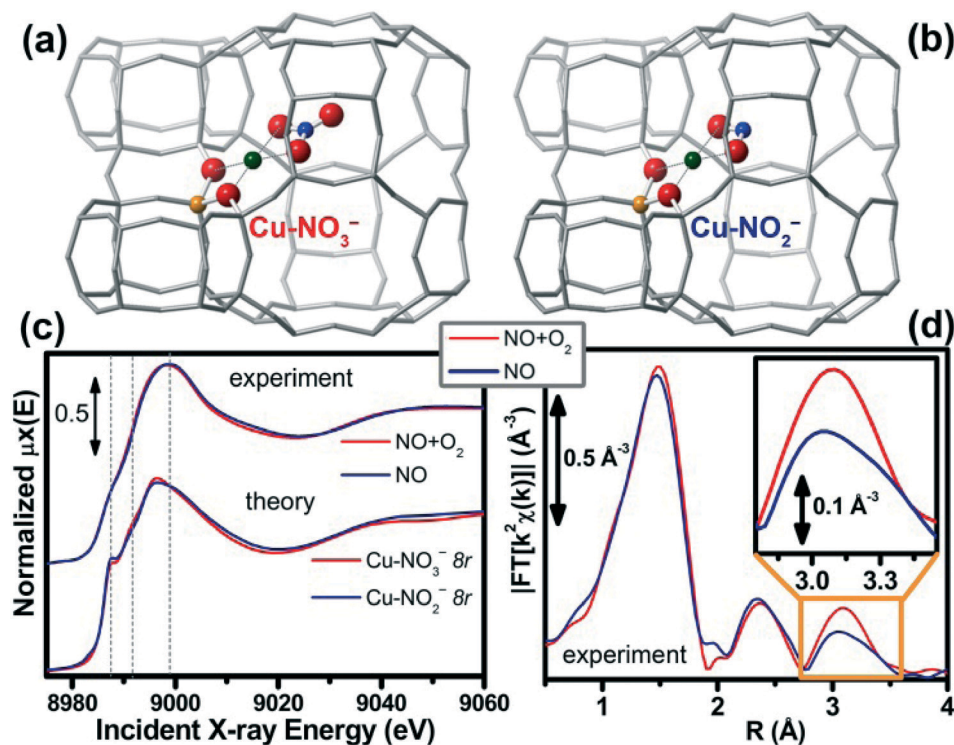


Fig. 3 DFT-optimized geometry of (a) $Cu(II)$ - NO_3^- and (b) $Cu(II)$ - NO_2^- complexes in the CHA framework in the vicinity of a single Al framework atom (1Al site). The zeolite framework is visualized by the grey wireframe, and the complexes are given as ball-stick models (Cu: green, Al: yellow, O: red and N: blue). In (c), the top curves show the experimental Cu K-edge XANES spectra obtained under the $NO + O_2$ feed (red line) and NO feed (blue line) measured at 100 °C. The bottom curves in (c) show simulated XANES spectra derived from the $Cu(II)$ - NO_3^- (red curve) and the Cu - NO_2^- 8r from the DFT-optimized geometries. (d) Phase-uncorrected $|FT[k^2\chi(k)]|$ curves obtained by Fourier transforming the $k^2\chi(k)$ spectra of the CHA catalyst under the $NO + O_2$ and NO -only conditions, reported with the same color code used in the top part of (c). The inset shows a magnification of the third maximum region, where the differences crucial for the discrimination between Cu -nitrates and Cu -nitrites species are observed.

the presence of adsorbed molecules.¹⁸ However, at the selected catalyst composition (Si/Al = 15 and Cu/Al = 0.48), Z-[Cu(II)OH⁺] complexes in the 8r have been established as the dominant Cu-species in the O₂-dehydrated state.^{9,11,17} Hence, Cu-species hosted at 1Al sites in the 8r have been selected for detailed EXAFS analysis, as discussed below.

The most likely configurations evidenced by our analysis are shown in Fig. 3a and b. As seen in Fig. 3c, the features in the XANES spectra are well described by the corresponding theoretical models. Interestingly, the energy positions of the major XANES transitions are better reproduced upon a 4% isotropic contraction from the DFT-optimized bond distances from the Cu-sites (see also Fig. S3b and c, ESI†). In agreement with our experimental observations, also theoretical XANES for Cu(II)-nitrate and presumed Cu(II)-nitrite species are very similar, which is not surprising considering the very similar coordination environment predicted by DFT.

Further insights into the reaction between NO and Cu(II)-nitrates can be obtained by looking at the FT-EXAFS spectra reported in Fig. 3d. Indeed, when Cu(II)-nitrates are exposed to NO, a notable decrease in the intensity of the maximum at *ca.* 3.1 Å in the phase-uncorrected FT-EXAFS spectra is observed, whereas for *R* < 3 Å the spectrum remains very similar to that of the NO + O₂ state. As discussed in detail in the following, the maximum at 3.1 Å in the FT-EXAFS is characteristic for the Cu-nitrate group. Thus, its intensity decrease indicates that the nitrate group has reacted with NO as already concluded on the basis of FTIR and UV-vis-NIR. Simultaneously, the similarity of the FT-EXAFS in the remaining *R*-range evidences that Cu-nitrates have been converted to Cu(II)-moieties with an equivalent geometry up to the second coordination sphere of Cu centers. Being aware that the high-*R* region in FT-EXAFS is inherently affected by lower sensitivity and possible Fourier transform artefacts, we carefully analyzed in *k*-space the raw *k*²-weighted $\chi(k)$ spectra collected with the NO + O₂ feed and NO-only feed (see section 4.3, ESI†), concluding that the observed differences are physically significant.

According to eqn (1), the reaction between NO and Cu(II)-NO₃⁻ should produce a Cu(II)-NO₂⁻ group and an NO₂ molecule in the gas phase. Indeed, transient formation of NO₂ has been observed upon exposure of Cu-zeolites containing nitrates to an NO atmosphere, supporting the formation of Cu(II)-nitrites.²³ To investigate the possibility of this Cu(II)-nitrite formation, the EXAFS data collected in the NO-only state were therefore refined assuming that Cu-nitrite species are formed to some extent.

The EXAFS analysis is based on the DFT-optimized structure models (Fig. 3a and b and 4a and d) that are further refined to fit the data. For strategy and details of the refinements, please see section 4 of the ESI†. In the following sections, the Cu(II)-nitrate phase formed after exposure to NO + O₂ at 200 °C is first characterized in detail by EXAFS. Then, the possible formation of a Cu(II)-nitrite species upon exposure of the Cu(II)-nitrate to NO is investigated.

Fig. 4a–c show the Cu(II)-NO₃⁻ structure hosted in the 8r of the CHA framework as suggested by DFT and the *k*²-weighted Fourier transform of the EXAFS data (both the magnitude and the imaginary part) collected in the NO + O₂ state. The magnitude of the FT for the Cu(II)-nitrate species shows maxima at *ca.* 1.4 Å, 2.4 Å and 3.1 Å. As evidenced by DFT-assisted EXAFS fitting, the maximum at *ca.* 2.4 Å derives from Cu–Al SS paths, typical for Cu(II) ions located in the proximity of a framework Al atom, bound to the oxygen atoms of the zeolite framework.^{7,11,17,44} The maximum at *ca.* 3.1 Å originates from unusually strong collinear multiple scattering (MS) paths involving the nitrogen atom and the oxygen atom in the nitrate group pointing away from the Cu atom; the single scattering (SS) path involving this O atom has only a minor contribution. The collinear MS paths indicate that the Cu, N, and O atoms lie on an approximately straight line and are unique to the bidentate Cu(II)-nitrate species.

This fit ensured an excellent reproduction of the experimental spectrum, yielding physically meaningful parameter values (Table 1), indicating that the structure of the Cu(II)-nitrate found with DFT is in good agreement with the EXAFS data. The refined interatomic distances from the Cu center reported in Table 1 are in good agreement with the DFT-derived distances (see Fig. 4a), albeit slightly shortened. Remarkably, the overall shortening of bond distances found from the EXAFS fit is in line with XANES simulations, ensuring an improved reproduction of the experimental spectra in correspondence with a slight isotropic contraction of the DFT-optimized geometries, as mentioned above.

The structural models for the bidentate Cu(II)-nitrite species used as input for the refinement are shown in Fig. 3b and 4d. The absence of the collinear multiple scattering paths in the nitrite group results in a lower magnitude in the maximum of the FT(*R*) EXAFS spectrum at 3.1 Å. However, the magnitude of this peak observed for the measured data is higher than that expected for the presence of Cu-nitrites only (blue curve, Fig. 4e). This supports the partial conversion of nitrates to nitrites, as was also indicated by FTIR (Fig. 1). A two-component fit was performed to estimate the relative amounts of nitrate and nitrite species (see also section 4.2 of the ESI† for additional details). The best fitting to the experimental data was obtained having about 60% Cu(II)-nitrite and 40% Cu(II)-nitrate (see Table 1 and Fig. 4e and f), in qualitative agreement with the reduction in intensity in the FTIR bands of Cu(II)-nitrates by about 50% (Fig. 1). More specifically, from FTIR, the initial intensity of the nitrate band decreases by *ca.* 25% after 1 h at 200 °C in NO, whereas stabilization at *ca.* 50% of the initial intensity is observed after *ca.* 2 h (see Fig. 1b). An equivalent result (stabilized signal, assigned to *ca.* 50% Cu-nitrate and 50% Cu-nitrite species) is found by XAS already after 1 h of exposure at 200 °C. However, it is important to note that a direct, quantitative, comparison between the time scale of FTIR experiments and either XAS or UV-vis ones is not straightforward (see also section 1, ESI†), due to the different experimental conditions employed, specifically optimized for each

Table 1 Best-fit values for the parameters optimized by fitting the k^2 -weighted spectrum of Cu-CHA under the NO + O₂ feed and NO feed (data collected at 100 °C), employing DFT-derived Cu(II)-NO₃⁻ and Cu(II)-NO₂⁻ geometries as starting guesses (see Fig. 4a and d). Fits were performed in *R*-space in the range of 1.0–3.8 Å, employing the *k*-range of 2.5–12.4 Å⁻¹ for the FT, resulting in a number of independent points $2\Delta k\Delta R/\pi > 18$. The underlined parameters have been set to fixed values in the fit. In particular, the amplitude S_0^2 was set to 0.9 on the basis of the analysis of a CuO reference; the distances R_N and $R_{O_2(NO_2)}$ were derived from the first shell distance R_{O1} on the basis of geometrical considerations (see section 4, ESI), allowing one to limit the number of parameters employed in the fitting model

	Fit parameters	NO + O ₂	NO-only ^a
	S_0^2	<u>0.9</u>	<u>0.9</u>
	ΔE (eV)	-3.7 ± 1.4	-3.8 ± 1.0
	<i>R</i> -factor	0.005	0.003
	No. fit par. ^b	11	12
Coordination to the Cu-CHA framework	#NO ₃	<u>1.0</u>	0.4 ± 0.2
	$\langle R_{O(fw)} \rangle$ (Å)	1.92 ± 0.02	1.90 ± 0.02
	$\sigma_{O(fw)}^2$ (Å ²)	0.004 ± 0.002	0.003 ± 0.001
	R_{Al} (Å)	2.76 ± 0.01	2.76 ± 0.01
	σ_{Al}^2 (Å ²)	0.003 ± 0.001	0.005 ± 0.002
	α_{fw}	-0.02 ± 0.01	-0.05 ± 0.01
Coordination to NO ₃ ⁻ /NO ₂ ⁻ groups	σ_{fw}^2 (Å ²)	0.013 ± 0.004	0.008 ± 0.002
	$\langle R_{O1} \rangle$ (Å)	1.98 ± 0.01	1.99 ± 0.01
	σ_{O1}^2 (Å ²)	0.006 ± 0.004	0.006 ± 0.003
	R_N (Å)	<u>2.38</u>	<u>2.40</u>
	σ_N^2 (Å ²)	0.004 ± 0.003	0.007 ± 0.004
	$R_{O_2(NO_2)}$ (Å)	<u>3.60</u>	<u>3.61</u>
	$\sigma_{MS(NO_2)}^2$ (Å ²)	0.004 ± 0.002	0.005 ± 0.003

^a Experimental spectrum fitted as follows: $\#_{NO_3} \cdot \{FT[k^2\chi(k)_{Cu-NO_3}]\} + (1 - \#_{NO_3}) \cdot \{FT[k^2\chi(k)_{Cu-NO_2}]\}$; $(1 - \#_{NO_3}) = \#_{NO_2}$. ^b The high similarity of the Cu(II)-NO₃ and the Cu(II)-NO₂ DFT geometries (see Fig. 4a and d) allowed us to use only one extra parameter in the 2-component fit employing a common set of parameters for both components (see section 4.2 of the ESI for details). In both cases, the number of free parameters (11 and 12 for 1- and 2-component fits, respectively) is well below the number of independent points ($2\Delta k\Delta R/\pi > 18$).

spectroscopy (different sample mass, powdered or pelletized sample, gas flow passing or not through the sample).

2.4 Verifying the coordinative nature of nitrite species by EXAFS

The bidentate Cu-nitrite species used for refinement (Fig. 4d) was not the only viable nitrite species structure offered by DFT. When screening for possible nitrite species, DFT was unable to rule out the possibility of having monodentate coordination, with Cu coordinating to the N-side of the nitrite (Fig. 5a), instead of the bidentate coordination seen in Fig. 4d. However, the coordination environment of the monodentate nitrite species proposed by DFT is drastically different with respect to the chelating bidentate Cu-nitrates, established to be the major structural component in the NO + O₂ state. The high similarity of the EXAFS spectra measured under the NO + O₂ and the NO-only conditions, in relation to the first and second coordination shells, therefore qualitatively discourages the presence of major contributions from monodentate Cu-nitrites.

Simulated XANES spectra for monodentate Cu-nitrites also show significantly worse agreement with the experimental curves with respect to the bidentate configurations (see Fig. S3, ESI†). Moreover, EXAFS simulations and tentative refinements using monodentate Cu-nitrite geometries showed to be fully inadequate to reproduce the observed data (Fig. 5 and section 5, ESI†). Based on this, the possibility of having

monodentate nitrite species as a major nitrite species during the reaction between nitrate ligands and NO can be ruled out. This result is also in agreement with the similar spectral features observed by UV-vis-NIR when nitrate (NO + O₂) and nitrite (NO at 100 °C) are formed (Fig. 2).

2.5 Final remarks on the formation of Cu-nitrite species

The results presented above clearly indicate that a reaction takes place between Cu-nitrate and NO. This indicates that the reaction step given in eqn (1) actually can occur and is in agreement with the observation of a transient formation of NO₂ to the gas phase.^{7,22} Evidence that this reaction can proceed in both directions is supported by the observation that exposure of a Cu-nitrate to NO results in a transient formation of gaseous NO₂, while exposure of a Cu-zeolite to NO₂ results in a transient formation of gaseous NO.^{20,22}

Having established that the reaction occurs, the reaction must at least involve the detachment of an oxygen atom of the nitrate group and the attachment to an NO molecule. Several ways of doing this can be envisaged. Based on the conclusion that both the Cu-nitrate and Cu-nitrite show a bidentate configuration, it could be argued that the reaction of NO with nitrate – and the reverse reaction, the formation of nitrate from nitrite + NO₂ – proceeds *via* direct detachment or attachment of the oxygen atom pointing away from the Cu ion in the Cu-nitrate group. This would then be a direct reaction between the Cu ligands and gas phase molecules, and

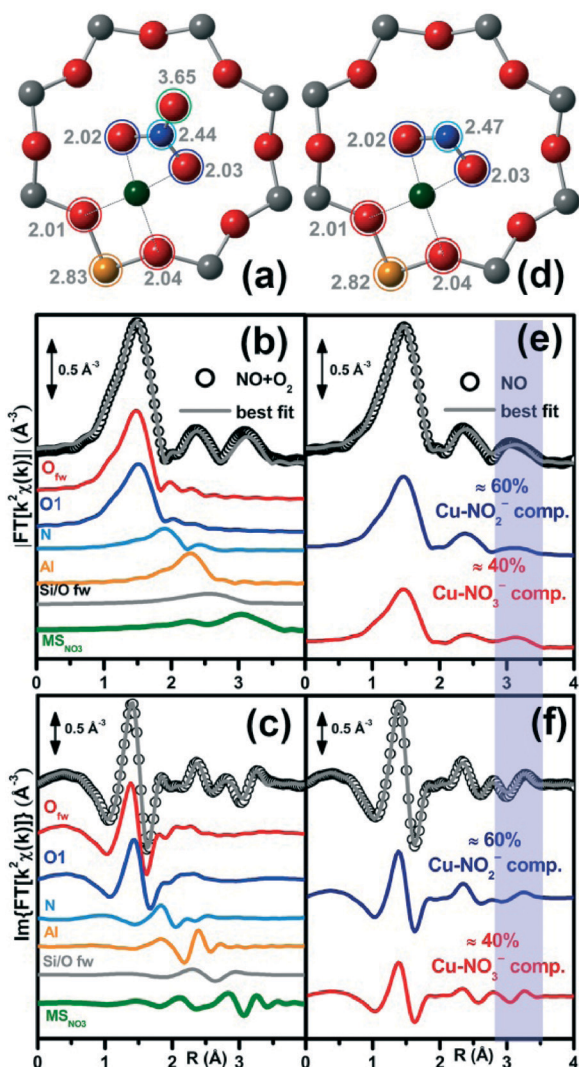


Fig. 4 (a and d) DFT-optimized geometry of the (a) Cu(II)-NO₃⁻ and (d) Cu(II)-NO₂⁻ chelating bidentate complexes hosted in the 8r unit of the CHA framework with distances from Cu by DFT expressed in Å. Atom colour code: Cu (absorber): green; O: red; N: blue; Si: grey; Al: orange. Magnitude (b and e) and imaginary parts (c and f) of the experimental FT EXAFS spectra (black circles) and the corresponding best fit curves (solid grey lines), obtained under the NO + O₂ feed (b and c) and NO feed (e and f). Different SS and MS path contributions to the EXAFS signal of Cu(II)-NO₃⁻ species are shown in parts (b) and (c) with colours corresponding to the involved atoms highlighted in part (a). (d and f) Individual phase contributions from Cu(II)-NO₂⁻ (blue) and Cu(II)-NO₃⁻ (red) complexes.

the influence of the Cu ion would be limited, as the reaction does not involve breaking or creating bonds to the Cu ions.

Another possible pathway is based on partial reversal of the Cu-nitrate formation by the reaction of O₂ and NO on a Cu(I) ion. DFT calculations have shown that the formation of nitrates from NO occurs by sequential incorporation of the oxygen atoms from the O₂ molecule in the NO molecule.⁴⁵ The incorporation of the first oxygen atom is endothermic (+0.85 eV) and leads to a first intermediate state of the nitrate formation with a linearly bound NO₂ moiety and an oxygen

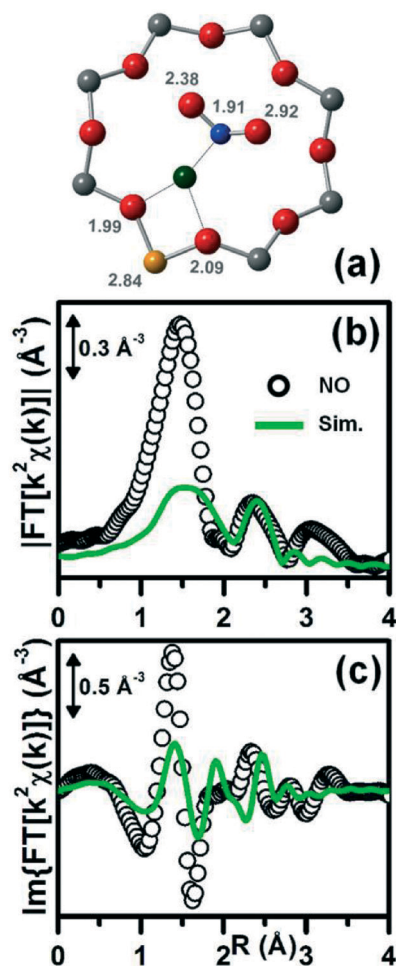


Fig. 5 (a) DFT-optimized geometry of the hypothetical Cu(II)-NO₂⁻ monodentate complex hosted in the 8r unit of the CHA framework with distances from Cu given by DFT expressed in Å. Atom colour code: Cu (absorber): green; O: red; N: blue; Si: grey; Al: orange. Magnitude (b) and imaginary part (c) of the experimental FT EXAFS spectra (black circles) obtained under the NO feed and corresponding simulation curves (solid green lines) based on the structure shown in (a). See section 4 of the ESI† for details.

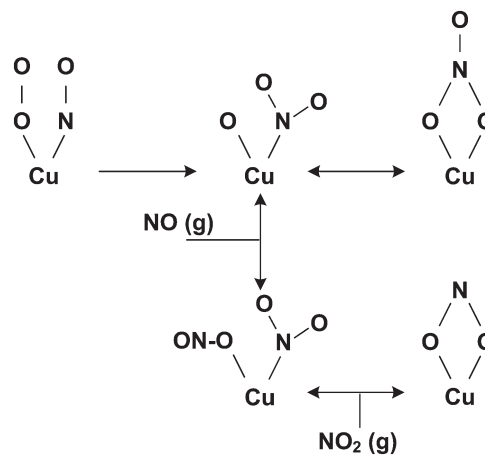


Fig. 6 Proposed reaction scheme for the reaction of NO(g) + Cu-nitrate to Cu-nitrite and NO₂(g).

atom. The bidentate nitrate is then formed by the exothermic incorporation of the second oxygen atom. If the second step of the nitrate formation is reversed in the presence of NO, then it can be envisaged that the single oxygen atom attached to the Cu ion reacts with NO to form NO₂, followed by a rearrangement of the linearly bound nitrite group to a bidentate configuration, as displayed in the reaction scheme in Fig. 6. Such a reaction pathway would be strongly influenced by the Cu ions, as it involves bond breaking and formation directly to the Cu ions in the zeolite.

It is noted that Cu-nitrate is the most stable configuration shown in Fig. 6, and it is converted under NH₃-SCR conditions.^{7,45} The stability of the Cu-nitrate is the reason why it is so prominent in spectroscopy. Nevertheless, the role of the nitrate in the NH₃-SCR reaction may, according to the reaction scheme, be limited, as the reactivity of the nitrate species towards NO depends on the ability to form an activated state, which actually interacts with the reaction gas in the NH₃-SCR reaction (either NO or NH₃). In that case, the Cu-nitrate species itself is not really active in the NH₃-SCR reaction but is able to form an active state; Cu-nitrate can be thus regarded as a supplier of active species. Such a scenario also accounts for both the appearance of Cu-nitrates in spectroscopy and the fact that it disappears under NH₃-SCR conditions in an atmosphere containing NH₃ and NO.⁷

Finally, in Fig. 1, it is shown that at 200 °C about 50% of the Cu-nitrate is converted by NO in about 2.5 h, which seems much slower than the very fast NH₃-SCR reaction. A possible reason for this discrepancy is that in the experiments shown in this article, no NH₃ is present. It has been shown earlier that the presence of both NO and NH₃ leads to a very fast conversion of Cu-nitrate to a Cu(I) species.⁷ When no NH₃ is present, this very fast reduction cannot occur, and therefore, slower reactions that can occur between Cu-nitrate and Cu-nitrite with NO_x become more prominent, as they no longer compete with the very fast reduction by the mixture of NH₃ and NO. It is also possible that Cu-nitrites are converted back to Cu-nitrate,²⁷ leading to partial conversion of Cu-nitrate as it is observed here. In conclusion, the absence of the very fast reduction in a mixture of NO and NH₃, which is present in NH₃-SCR, causes other, slower reactions to prevail.

3. Experimental

3.1 Synthesis

The Cu-CHA sample was prepared using a method similar to that reported earlier.⁸ A synthesis gel with the composition 1.0 Si/0.0667 Al/0.5 TMAdaOH/0.5 HF/3 H₂O was prepared by dissolving aluminum isopropoxide (98%, Sigma-Aldrich) in tetraethyl orthosilicate (98% Aldrich) and adding *N,N,N*-trimethyladamantammonium hydroxide (TMAdaOH, 25 wt%, Sachem) to the solution. This mixture was stirred to homogenize overnight. Hydrofluoric acid (48 wt%, 99.99% trace-metal basis, Sigma-Aldrich) was added, and the mixture was stirred by hand. Water was evaporated from the gel at 60 °C

by regular manual homogenization until the desired content was obtained. To form the CHA zeolite, the gel was heated to 150 °C for 3 days under rotation in a Teflon-lined autoclave. The CHA product was recovered by filtration and washed several times with water, followed by calcination at 580 °C for 3 h to remove the TMAdaOH. Copper ions were introduced by suspending the calcined CHA in 250 ml per g_{zeolite} of 5 mM copper(II) acetate solution and stirred at room temperature (RT) for 24 h. Finally, the product was filtered, washed, and calcined in air at 500 °C for 3 h. The final Cu-CHA obtained and used in this work had Si/Al = 15 and Cu/Al = 0.48, corresponding to a Cu content of 2.6 wt%. The NH₃-SCR activity of this catalyst can be found in Fig. 1 of ref. 7.

3.2 Density functional theory (DFT) calculations

Spin-polarized DFT calculations were used to optimize the geometry of Cu(II)-NO₃⁻ and Cu(II)-NO₂⁻ species hosted in both the 8r and the 6r units of the CHA framework. The optimized structures were used as input for the analysis of the XAS data. The calculations were performed with the GPAW package^{46,47} using a real space grid-based projector augmented wave method. A grid spacing of $h = 0.2$ and a Fermi smearing of 0.1 K were found sufficient to obtain a satisfactory convergence of the relative energies. The BEEF-vdW functional⁴⁸ was used to account for the van der Waals interactions. The zeolite was represented by periodic cells with hexagonal symmetry (cell parameters $a, b = 13.886$ Å; $c = 15.116$ Å; $\alpha = 120^\circ$; $\beta, \gamma = 90^\circ$), containing 36 T atoms.

3.3 X-ray absorption spectroscopy (XAS)

3.3.1 XAS experimental setup. The XAS experiment was performed at beamline I811, MAX-lab (Sweden).⁴⁹ The sample was measured at the Cu K-edge in transmission mode using a double Si(111) crystal monochromator with a detuning of -20%. The X-ray beam was set to a size of 0.5×0.5 mm². A copper foil was measured simultaneously with a third detector for energy calibration. Continuous scans were performed in the range of 8830–10 180 eV with an equidistant energy spacing of 0.2 eV and a constant sampling time of 0.05 s at each energy point; the time for a single scan was 6 min. By averaging 10 continuous scans taken at 100 °C, EXAFS data with sufficient quality for quantitative analysis were obtained.

For the *in situ* XAS measurements, a sample of 65 mg of the Cu-CHA catalyst was loaded into an in-house designed cell,⁵⁰ in which the gas atmosphere, temperature and pressure were controlled during the experiment. The gas flow applied was 50 Nml min⁻¹ in the entire experiment. For activation, the sample was heated at 500 °C for 30 min in technical air.^{8,11} Then, to form the Cu(II)-nitrate species, the sample was exposed to 500 ppm NO, 10% O₂ in N₂ at 200 °C,⁷ and then the temperature was lowered temporarily to 100 °C for high-quality spectra acquisition (NO + O₂ conditions). To monitor the reaction between NO and the nitrate phase, the gas was changed to a feed of 500 ppm NO in N₂ (without

oxygen: NO-only conditions) at the same temperature, heated to 200 °C for approximately one hour before being cooled again to 100 °C for high-quality spectra acquisition. Moreover, such an acquisition protocol is expected to maximize the population of possible Cu-nitrite species. Indeed, according to FTIR (see section 2.1), Cu-nitrates are converted more efficiently at 200 °C and subsequent cooling to 100 °C should limit the possible thermal decomposition of Cu-nitrites.

3.3.2 EXAFS data analysis. The averaged EXAFS spectra measured at 100 °C for both the NO + O₂ and the NO-only conditions were fitted in *R*-space in the $\Delta R = 1.0\text{--}3.8$ Å range, considering the FT of the k^2 -weighted $\chi(k)$ EXAFS spectrum, and Fourier transformed in the 2.5–12.4 Å⁻¹ range, resulting in 18 independent points ($2\Delta k\Delta R/\pi > 18$). Phases and amplitudes were calculated by the FEFF6 code^{51,52} using the Artemis software from the Demeter package.⁵³ Structures obtained from DFT analysis of Cu(II)-nitrates and Cu(II)-nitrites in the 8r units of the CHA framework were adopted as inputs for the FEFF calculations, to set the coordination numbers and provide initial guesses for the bond distances. In the fitting model, all the single-scattering (SS) paths contributing to the *R*-space interval of interest and the principal multiple-scattering (MS) contributions were included (see section 4, ESI†).

3.3.3 XANES simulations. Cu K-edge XANES simulations were performed using the optimized DFT structures for Cu(II)-NO₃⁻ and Cu(II)-NO₂⁻ in the CHA zeolite by the FDMNES code,^{54,55} which was recently considerably sped up.^{56,57} The calculations were carried out using a finite difference method without restrictions on the potential shape, which allowed one to account for the anisotropy of the coordination environment of the absorbing atom in the CHA structure. The calculations were performed on a discrete grid of points, mapped inside a sphere with a radius of 5 Å, centered at the absorbing Cu atom. Constant Gaussian and energy-dependent Lorentzian broadenings were applied in order to account for instrumental resolution, Cu core-hole lifetimes and other broadening effects.

3.4 Fourier transform infrared spectroscopy (FTIR)

The FTIR spectra were recorded in transmission mode with a resolution of 2 cm⁻¹ on a PerkinElmer System 2000 infrared spectrophotometer equipped with an MCT detector at liquid nitrogen temperature. For the *in situ* FTIR measurements, approximately 15 mg of the Cu-CHA catalyst was pressed into a self-supported pellet and placed inside a commercial FTIR reactor cell (AABSPEC, no. 2000-A multimode) with controlled gas atmosphere and temperature. The gas flow used in the experiments was 50 ml min⁻¹. The catalyst was first heated at 400 °C for 60 min (heating rate 5 °C min⁻¹) in a mixture of 10% O₂ in He. Then, the sample was cooled to 200 °C and exposed to a mixture of 1000 ppm NO and 10% O₂ in He, to form the Cu(II)-nitrate species. The reaction between NO and nitrate was monitored at 200, 150 and 100 °C by removing O₂ from the feed gas.

3.5 UV-visible-NIR spectroscopy (UV-vis-NIR)

UV-vis-NIR absorption spectra of Cu-CHA were recorded using an Agilent UV-vis-NIR Cary 5000 spectrometer equipped with a diffuse reflectance attachment with an integrating sphere. Prior to each measurement, a baseline spectrum was collected from a Teflon reference sample. The spectra were collected between 50 000 and 4000 cm⁻¹ with 10 cm⁻¹ intervals at 6000 cm⁻¹ min⁻¹. About 0.4 gram of Cu-CHA was introduced into an in-house designed quartz cell. Prior to measurements, the sample was heated at 400 °C for 1 h in a dry 10% O₂/He gas mixture. Then, the sample was exposed to a mixture of 1000 ppm NO and 10% O₂ in He at 200 °C, to form the Cu(II)-nitrate, and subsequently to 1000 ppm NO in He at 200 °C or 100 °C. The total gas flow was 50 ml min⁻¹ in all measurements. UV-vis spectra were obtained by closing the cell and cooling the sample to room temperature after each step.

4. Conclusions

The reaction between NO and nitrate species in a Cu-CHA catalyst was studied by FTIR, UV-vis spectroscopy, and XAS supported by DFT. Heating a Cu-CHA catalyst in oxygen results in dehydration, while preserving the Cu(II) oxidation state. Exposure of the oxidized Cu-CHA catalyst to a mixture of NO and O₂ at 200 °C leads to the formation of a bidentate Cu(II)-nitrate species. When this Cu(II)-nitrate species is further exposed to NO in the absence of O₂, between 100 °C and 200 °C, partial conversion (about 50%) of the nitrate species is observed. The state of the catalyst at this stage is different from the original oxidized Cu-CHA catalyst. A detailed structural analysis of the Cu coordination environment based on XAS data reveals a state that is consistent with the conversion of about half of the Cu(II)-nitrate to a bidentate Cu(II)-nitrite species; formation of a monodentate N-bound Cu-nitrite species is ruled out. This indicates that a reaction of Cu(II)-nitrate with NO occurs, supporting the hypothesis that conversion of nitrates to nitrites can indeed partake in the NH₃-SCR reaction in Cu-CHA.

Acknowledgements

Robin Christensen, Lone Bech, David N. McCarthy and Lars F. Lundegaard from Haldor Topsoe A/S and Stefan Carlson, a beamline scientist at I811 (MAX-lab), are thanked for their assistance during the XAS experiments. Mariia A. Volkova from Ivanovo State University of Chemistry and Technology (Russian Federation) and Anita Godiksen from Technical University of Denmark are kindly acknowledged for contributing to infrared and UV-vis-NIR measurements. CL and KAL acknowledge the Megagrant of the Russian Federation Government to support scientific research at the Southern Federal University, no. 14.Y26.31.0001. KAL acknowledges the scholarship of the President of Russia for Ph.D. students and young scientists no. CIP-2796.2016.1. EB acknowledges Innovation Fund Denmark (Industrial postdoc n. 5190-00018B).

Notes and references

- 1 A. M. Beale, F. Gao, I. Lezcano-Gonzalez, C. H. F. Peden and J. Szanyi, *Chem. Soc. Rev.*, 2015, **44**, 7371–7405.
- 2 D. W. Fickel, E. D'Addio, J. A. Lauterbach and R. F. Lobo, *Appl. Catal., B*, 2011, **102**, 441–448.
- 3 J. H. Kwak, R. G. Tonkyn, D. H. Kim, J. Szanyi and C. H. F. Peden, *J. Catal.*, 2010, **275**, 187–190.
- 4 F. Gao, J. Kwak, J. Szanyi and C. F. Peden, *Top. Catal.*, 2013, **56**, 1441–1459.
- 5 A. Boubnov, H. W. P. Carvalho, D. E. Doronkin, T. Günter, E. Gallo, A. J. Atkins, C. R. Jacob and J.-D. Grunwaldt, *J. Am. Chem. Soc.*, 2014, **136**, 13006–13015.
- 6 D. E. Doronkin, M. Casapu, T. Günter, O. Müller, R. Frahm and J.-D. Grunwaldt, *J. Phys. Chem. C*, 2014, **118**, 10204–10212.
- 7 T. V. W. Janssens, H. Falsig, L. F. Lundegaard, P. N. R. Vennestrom, S. B. Rasmussen, P. G. Moses, F. Giordanino, E. Borfecchia, K. A. Lomachenko, C. Lamberti, S. Bordiga, A. Godiksen, S. Mossin and P. Beato, *ACS Catal.*, 2015, **5**, 2832–2845.
- 8 F. Giordanino, P. N. Vennestrom, L. F. Lundegaard, F. N. Stappen, S. Mossin, P. Beato, S. Bordiga and C. Lamberti, *Dalton Trans.*, 2013, **42**, 12741–12761.
- 9 C. W. Andersen, M. Bremholm, P. N. R. Vennestrom, A. B. Blichfeld, L. F. Lundegaard and B. B. Iversen, *IUCr*, 2014, **1**, 382–386.
- 10 A. Godiksen, F. N. Stappen, P. N. R. Vennestrom, F. Giordanino, S. B. Rasmussen, L. F. Lundegaard and S. Mossin, *J. Phys. Chem. C*, 2014, **118**, 23126–23138.
- 11 E. Borfecchia, K. A. Lomachenko, F. Giordanino, H. Falsig, P. Beato, A. V. Soldatov, S. Bordiga and C. Lamberti, *Chem. Sci.*, 2015, **6**, 548–563.
- 12 S. A. Bates, A. A. Verma, C. Paolucci, A. A. Parekh, T. Anggara, A. Yezerets, W. F. Schneider, J. T. Miller, W. N. Delgass and F. H. Ribeiro, *J. Catal.*, 2014, **312**, 87–97.
- 13 F. Gao, E. D. Walter, M. Kollar, Y. L. Wang, J. Szanyi and C. H. F. Peden, *J. Catal.*, 2014, **319**, 1–14.
- 14 F. Goltl and J. Hafner, *J. Chem. Phys.*, 2012, **136**, 064501.
- 15 F. Goltl and P. Sautet, *J. Chem. Phys.*, 2014, **140**, 154105.
- 16 F. Goltl, R. E. Bulo, J. Hafner and P. Sautet, *J. Phys. Chem. Lett.*, 2013, **4**, 2244–2249.
- 17 C. Paolucci, A. A. Parekh, I. Khurana, J. R. Di Iorio, H. Li, J. D. Albarracin Caballero, A. J. Shih, T. Anggara, W. N. Delgass, J. T. Miller, F. H. Ribeiro, R. Gounder and W. F. Schneider, *J. Am. Chem. Soc.*, 2016, **138**, 6028–6048.
- 18 R. Zhang, J. Szanyi, F. Gao and J.-S. McEwen, *Catal. Sci. Technol.*, 2016, **6**, 5812–5829.
- 19 K. A. Lomachenko, E. Borfecchia, C. Negri, G. Berlier, C. Lamberti, P. Beato, H. Falsig and S. Bordiga, *J. Am. Chem. Soc.*, 2016, **138**, 12025–12028.
- 20 D. Wang, L. Zhang, K. Kamasamudram and W. S. Epling, *ACS Catal.*, 2013, **3**, 871–881.
- 21 A. V. Kucherov, J. L. Gerlock, H.-W. Jen and M. Shelef, *Zeolites*, 1995, **15**, 9–14.
- 22 M. Colombo, I. Nova and E. Tronconi, *Catal. Today*, 2012, **197**, 243–255.
- 23 M. Colombo, I. Nova and E. Tronconi, *Catal. Today*, 2010, **151**, 223–230.
- 24 K. H. Stern, *J. Phys. Chem. Ref. Data*, 1972, **1**, 747–772.
- 25 V. A. Matyshak, N. V. Konokhov, V. F. Tret'yakov, Y. P. Tyulenin, O. N. Sil'chenkova, V. N. Korchak and R. Wong, *Kinet. Catal.*, 2011, **52**, 409–417.
- 26 M. Schramlmarth, A. Wokaun and A. Baiker, *J. Catal.*, 1992, **138**, 306–321.
- 27 L. Lietti, M. Daturi, V. Blasin-Aube, G. Ghiotti, F. Prinetto and P. Forzatti, *ChemCatChem*, 2012, **4**, 55–58.
- 28 M. P. Ruggeri, T. Selleri, M. Colombo, I. Nova and E. Tronconi, *J. Catal.*, 2014, **311**, 266–270.
- 29 C. Lamberti, A. Zecchina, E. Groppo and S. Bordiga, *Chem. Soc. Rev.*, 2010, **39**, 4951–5001.
- 30 S. Bordiga, C. Lamberti, F. Bonino, A. Travert and F. Thibault-Starzyk, *Chem. Soc. Rev.*, 2015, **44**, 7262–7341.
- 31 S. Bordiga, E. Groppo, G. Agostini, J. A. van Bokhoven and C. Lamberti, *Chem. Rev.*, 2013, **113**, 1736–1850.
- 32 J. A. van Bokhoven and C. Lamberti, in *X-Ray Absorption and X-ray Emission Spectroscopy: Theory and Applications*, ed. J. A. van Bokhoven and C. Lamberti, John Wiley & Sons, 2015, ch. 13.
- 33 K. I. Hadjiivanov, *Catal. Rev.: Sci. Eng.*, 2000, **42**, 71–144.
- 34 E. I. Solomon, D. E. Heppner, E. M. Johnston, J. W. Ginsbach, J. Cirera, M. Qayyum, M. T. Kieber-Emmons, C. H. Kjaergaard, R. G. Hadt and L. Tian, *Chem. Rev.*, 2014, **114**, 3659–3853.
- 35 N. Lehnert, U. Cornelissen, F. Neese, T. Ono, Y. Noguchi, K.-I. Okamoto and K. Fujisawa, *Inorg. Chem.*, 2007, **46**, 3916–3933.
- 36 F. Giordanino, E. Borfecchia, K. A. Lomachenko, A. Lazzarini, G. Agostini, E. Gallo, A. V. Soldatov, P. Beato, S. Bordiga and C. Lamberti, *J. Phys. Chem. Lett.*, 2014, **5**, 1552–1559.
- 37 J. H. Kwak, T. Varga, C. H. F. Peden, F. Gao, J. C. Hanson and J. Szanyi, *J. Catal.*, 2014, **314**, 83–93.
- 38 F. Xamena, P. Fisticaro, G. Berlier, A. Zecchina, G. T. Palomino, C. Prestipino, S. Bordiga, E. Giamello and C. Lamberti, *J. Phys. Chem. B*, 2003, **107**, 7036–7044.
- 39 C. Prestipino, G. Berlier, F. Xamena, G. Spoto, S. Bordiga, A. Zecchina, G. T. Palomino, T. Yamamoto and C. Lamberti, *Chem. Phys. Lett.*, 2002, **363**, 389–396.
- 40 C. Lamberti, G. T. Palomino, S. Bordiga, G. Berlier, F. D'Acapito and A. Zecchina, *Angew. Chem., Int. Ed.*, 2000, **39**, 2138–2141.
- 41 G. T. Palomino, P. Fisticaro, S. Bordiga, A. Zecchina, E. Giamello and C. Lamberti, *J. Phys. Chem. B*, 2000, **104**, 4064–4073.
- 42 C. Lamberti, S. Bordiga, M. Salvalaggio, G. Spoto, A. Zecchina, F. Geobaldo, G. Vlaic and M. Bellatreccia, *J. Phys. Chem. B*, 1997, **101**, 344–360.
- 43 I. Lezcano-Gonzalez, D. S. Wragg, W. A. Slawinski, K. Hemelsoet, A. Van Yperen-De Deyne, M. Waroquier, V. Van Speybroeck and A. M. Beale, *J. Phys. Chem. C*, 2015, **119**, 24393–24403.
- 44 J. S. McEwen, T. Anggara, W. F. Schneider, V. F. Kispersky, J. T. Miller, W. N. Delgass and F. H. Ribeiro, *Catal. Today*, 2012, **184**, 129–144.

- 45 H. Falsig, P. N. R. Vennestrøm, P. G. Moses and T. V. W. Janssens, *Top. Catal.*, 2016, **59**, 861–865.
- 46 J. Enkovaara, C. Rostgaard, J. J. Mortensen, J. Chen, M. Dulak, L. Ferrighi, J. Gavnholt, C. Glinsvad, V. Haikola, H. A. Hansen, H. H. Kristoffersen, M. Kuisma, A. H. Larsen, L. Lehtovaara, M. Ljungberg, O. Lopez-Acevedo, P. G. Moses, J. Ojanen, T. Olsen, V. Petzold, N. A. Romero, J. Stausholm-Møller, M. Strange, G. A. Tritsarlis, M. Vanin, M. Walter, B. Hammer, H. Hakkinen, G. K. Madsen, R. M. Nieminen, J. K. Nørskov, M. Puska, T. T. Rantala, J. Schiøtz, K. S. Thygesen and K. W. Jacobsen, *J. Phys.: Condens. Matter*, 2010, **22**, 253202.
- 47 J. J. Mortensen, L. B. Hansen and K. W. Jacobsen, *Phys. Rev. B: Condens. Matter Mater. Phys.*, 2005, **71**, 035109.
- 48 J. Wellendorff, K. T. Lundgaard, A. Møgelhøj, V. Petzold, D. D. Landis, J. K. Nørskov, T. Bligaard and K. W. Jacobsen, *Phys. Rev. B: Condens. Matter Mater. Phys.*, 2012, **85**, 235149.
- 49 S. Carlson, M. Clausen, L. Gridneva, B. Sommarin and C. Svensson, *J. Synchrotron Radiat.*, 2006, **13**, 359–364.
- 50 B. S. Clausen and H. Topsøe, *Catal. Today*, 1991, **9**, 189–196.
- 51 S. I. Zabinsky, J. J. Rehr, A. Ankudinov, R. C. Albers and M. J. Eller, *Phys. Rev. B: Condens. Matter Mater. Phys.*, 1995, **52**, 2995–3009.
- 52 J. J. Rehr and R. C. Albers, *Rev. Mod. Phys.*, 2000, **72**, 621–654.
- 53 B. Ravel and M. Newville, *J. Synchrotron Radiat.*, 2005, **12**, 537–541.
- 54 Y. Joly, *Phys. Rev. B: Condens. Matter Mater. Phys.*, 2001, **63**, 125120.
- 55 O. Bunău and Y. Joly, *J. Phys.: Condens. Matter*, 2009, **21**, 345501.
- 56 S. A. Guda, A. A. Guda, M. A. Soldatov, K. A. Lomachenko, A. L. Bugaev, C. Lamberti, W. Gawelda, C. Bressler, G. Smolentsev, A. V. Soldatov and Y. Joly, *J. Chem. Theory Comput.*, 2015, **11**, 4512–4521.
- 57 A. A. Guda, S. A. Guda, M. A. Soldatov, K. A. Lomachenko, A. L. Bugaev, C. Lamberti, W. Gawelda, C. Bressler, G. Smolentsev, A. V. Soldatov and Y. Joly, *J. Phys.: Conf. Ser.*, 2016, **712**, 012004.